J. Fluid Mech. (1991), *vol.* 230, *pp.* 667–691
Printed in Great Britain

Two-layer hydraulics with comparable internal wave speeds

By RICHARD WILLIAMS AND LAURENCE ARMI
Scripps Institution of Oceanography, La Jolla, CA 92093-0230, USA

(Received 5 March 1990 and in revised form 9 March 1991)

Two-layer hydraulics is developed for problems in which the moving layers can have stagnant layers above and below, the two internal wave modes can have comparable speeds and the total depth of the moving layers may vary. The general development allows both Boussinesq and non-Boussinesq problems to be studied. Solutions are presented in the Froude-number plane and the effect of different layer densities on the form of the solution space is shown. The theory is applied to two-layer plunging flows and a variety of controlled solutions are found. Solutions for the $2\frac{1}{2}$-layer theory and the plunging flow theory are demonstrated experimentally. Shear instability is often observed in the divergent section of the channel.

1. Introduction

Two-layer hydraulics problems occur in a variety of practical and geophysical situations. A thorough understanding of the two-layer system will also give insight into the hydraulics of continuously stratified fluid. Two-layer hydraulics for flows through a contraction or over a sill were explored by Armi (1986), and this analysis was applied to various two-layer exchange flows by Armi & Farmer (1986) and Farmer & Armi (1986). In all these papers, the two layers were assumed to be bounded below by a rigid surface and above by a rigid lid or a free surface and so only the slower internal wave mode plays a role in the flows. Armi (1986) also reviewed earlier work on internal hydraulics.

Here, a general two-layer hydraulics theory is developed for flows through a contraction. The flow geometry is shown in figure 1: the moving layers are bounded above and below by stagnant layers, the total depth of the two moving layers is allowed to vary, so there are two internal wave modes that play a role in the problem. The Boussinesq approximation is not used, so any density step can be treated. Wood (1968) found a special self-similar solution to this problem but full solutions have not been presented before. The general formulation of the problem presented here is also applied to the flow of two layers beneath a stagnant layer, a problem discussed by Wood (1970) and Lai & Wood (1975).

Since slowly varying hydraulically controlled flows are being sought, regularity conditions and the associated conditions for critical flow are examined. The approach used is similar to that of Armi (1986). The flows are parametrized in terms of the internal Froude numbers of each layer and solutions for flows with a fixed flow ratio (ratio of volume flux in the two moving layers) but variable reservoir layer depths are presented in the Froude-number plane. Since there are now two internal wave modes, the Froude-number plane has two critical lines. We explore the effect of changing the density of the stagnant layers on the solution curves and on the

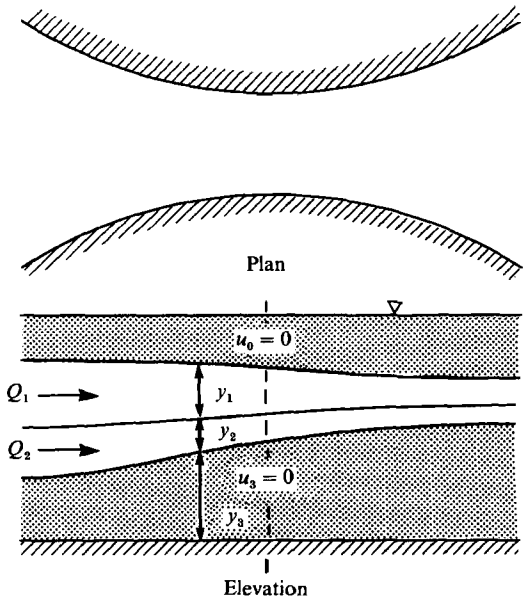

FIGURE 1. Two layers flowing through a contraction.

conditions for critical flow. The presentation in the Froude-number plane makes apparent the special nature of the self-similar solution.

We also consider flows in which the upper layer of the stagnant layers does not extend throughout the channel. These plunging flows occur when two layers flow into a reservoir of less dense fluid, and the flow rate is such that the lighter downstream reservoir fluid cannot extend back to the upstream reservoir. The flow leaving the upstream reservoir is governed by two-layer dynamics but at the downstream reservoir and for some distance into the contraction there is an overlying layer of stagnant fluid, and in this region the flow is governed by $2\frac{1}{2}$-layer dynamics. Single-layer flows of this type, termed 'box flows', were discussed by Armi & Farmer (1986) but the presence of two moving layers complicates the problem. The theory developed here is used to find hydraulically controlled two-layer plunging flows. Various flow regimes are found that allow controlled flows to occur at higher flow rates than Wood's self-similar solution permits.

The unidirectional flow through a contraction of two layers beneath a stagnation layer is also examined in a series of laboratory experiments. Flows with one and two controls and the extension at higher flow rates to plunging flows are demonstrated and compared with the theory.

2. Governing equations

The situation being considered is shown in figure 1. Two layers of fluid are moving through a contraction. They are bounded above and below by layers of stagnant fluid. The channel has vertical walls and the breadth is slowly varying. The bottom can be of any shape as long as it does not come into contact with the moving fluid. It is assumed that there is a steady, frictionless, one-dimensional hydrostatic flow. This flow is described by Bernoulli equations for the two moving layers and the lower stationary layer:

$$\tfrac{1}{2}\rho_1 u_1^2+(\rho_1-\rho_0)\,g(y_1+y_2+y_3)=(\rho_1-\rho_0)\,g(Y_1+Y_2+Y_3), \tag{1a}$$

$$\tfrac{1}{2}\rho_2 u_2^2+(\rho_1+\rho_0)\,gy_1+(\rho_2-\rho_0)\,g(y_2+y_3)=(\rho_1-\rho_0)\,gY_1+(\rho_2-\rho_0)\,g(Y_2+Y_3), \tag{1b}$$

$$(\rho_1-\rho_0)\,gy_1+(\rho_2-\rho_0)\,gy_2+(\rho_3-\rho_0)\,gy_3=(\rho_1-\rho_0)\,gY_1+(\rho_2-\rho_0)\,gY_2+(\rho_3-\rho_0)\,gY_3, \tag{1c}$$

where u_i, y_i, ρ_i and Y_i are respectively the velocity, thickness, density and upstream reservoir thickness of each layer. Subscript zero refers to the topmost layer and subscript three to the deepest layer. When (1*c*) is used to eliminate y_3 from (1*a*, *b*), the following are obtained:

$$\tfrac{1}{2}u_1^2+g\left(\frac{1-r_{01}}{1-r_{03}}\right)[y_1(1-r_{13})+y_2(1-r_{23})]=E_1. \tag{2a}$$

$$\tfrac{1}{2}u_2^2+g\left(\frac{1-r_{23}}{1-r_{03}}\right)[y_1(r_{12}-r_{02})+y_2(1-r_{02})]=E_2, \tag{2b}$$

where

$$r_{ij}=\rho_i/\rho_j \tag{2c}$$

and

$$E_1=g\left(\frac{1-r_{01}}{1-r_{03}}\right)[Y_1(1-r_{13})+Y_2(1-r_{23})], \tag{2d}$$

$$E_2=g\left(\frac{1-r_{23}}{1-r_{03}}\right)[Y_1(r_{12}-r_{02})+Y_2(1-r_{02})]. \tag{2e}$$

One or both stagnant layers can be removed by setting r_{0j} (no upper layer) or r_{i3} (no lower layer) equal to zero. Mass conservation is imposed by the requirement that the volume flow rate in each layer be constant:

$$Q_i=u_i y_i b, \tag{3}$$

where b is the channel width and Q_i is the layer volume flow rate, which is independent of streamwise location.

2.1. *Critical flow and regularity of solutions*

The following analysis is similar to that of Armi (1986). It is useful to define the Froude number for each layer by

$$\mathscr{F}_i^2=\frac{u_i^2}{g_i' y_i}, \tag{4a}$$

$$g_i'=g(1-r_{i-1,i})\,(1-r_{i,i+1}). \tag{4b}$$

This Froude number differs from those used in earlier works on two-layer hydraulics. It is motivated by a desire to use a Froude number that contains information about the layers both above and below the layer under consideration and leads to considerable simplification of the analysis and of the resulting equations. The more commonly used internal Froude number is defined by replacing g_i' in (4*a*) by $g'=g(1-r_{12})$:

$$F_i^2=\frac{u_i^2}{g' y_i}. \tag{4c}$$

A matrix formulation analogous to that used by Armi (1986) is found by taking the streamwise (x) derivative of ($2a$, b) and (3):

$$\boldsymbol{C}\boldsymbol{v}_x = \boldsymbol{D}f_x$$

where

$$\boldsymbol{C} = \begin{bmatrix} u_1 & 0 & \dfrac{(1-r_{01})(1-r_{13})}{1-r_{03}}g & \dfrac{(1-r_{01})(1-r_{23})}{1-r_{03}}g \\ 0 & u_2 & \dfrac{(1-r_{23})(r_{12}-r_{02})}{1-r_{03}}g & \dfrac{(1-r_{23})(1-r_{02})}{1-r_{03}}g \\ y_1 & 0 & u_1 & 0 \\ 0 & y_2 & 0 & u_2 \end{bmatrix},$$

$$\boldsymbol{D} = \begin{bmatrix} 0 \\ 0 \\ Q_1 \\ Q_2 \end{bmatrix}, \quad v = \begin{bmatrix} u_1 \\ u_2 \\ y_1 \\ y_2 \end{bmatrix}, \quad f = [b^{-1}]$$

and the subscript x denotes streamwise differentiation. These equations are solved for the u_{ix} in terms of the Froude numbers and the independent topographic variable b:

$$\frac{u_{1x}}{u_1} = \frac{b_x}{b}\left[\frac{(1-r_{13}+(1-r_{23})\,y_2/y_1)\,\mathscr{F}_2^2-1}{1-G^2}\right], \tag{5a}$$

$$\frac{u_{2x}}{u_2} = \frac{b_x}{b}\left[\frac{(1-r_{02}+(r_{12}-r_{02})\,y_1/y_2)\,\mathscr{F}_1^2-1}{1-G^2}\right], \tag{5b}$$

where G^2 is a new composite Froude number,

$$G^2 = \mathscr{F}_1^2(1-r_{02})-\mathscr{F}_2^2(1-r_{13})-\mathscr{F}_1^2\mathscr{F}_2^2(1-r_{12})\,(1-r_{03}). \tag{6}$$

The flow is critical when $G^2 = 1$, and solutions to ($5a$, b) are well behaved only if the numerators also vanish:

$$\frac{b_x}{b}[(1-r_{13}+(1-r_{23})\,y_2/y_1)\,\mathscr{F}_2^2-1] = 0, \tag{7a}$$

$$\frac{b_x}{b}[(1-r_{02}+(r_{12}-r_{02})\,y_1/y_2)\,\mathscr{F}_1^2-1] = 0. \tag{7b}$$

These regularity conditions are always satisfied at the narrowest section, where $b_x = 0$. When $b_x \neq 0$, ($7a$, b) can be solved to find that

$$\frac{\mathscr{F}_1^2}{\mathscr{F}_2^2} = \frac{y_2}{y_1}\left[\frac{(1-r_{13})\,y_1+(1-r_{23})\,y_2}{(r_{12}-r_{02})\,y_1+(1-r_{02})\,y_2}\right]. \tag{8}$$

When this condition holds, there is a control at some section other than the narrowest section. This result was first found by Wood (1968), and the control was called a virtual control. The special character of solutions with a virtual control can be seen by solving the Bernoulli equations ($2a$, b) for the moving layers for the Froude-number ratio of the flow,

$$\frac{\mathscr{F}_1^2}{\mathscr{F}_2^2} = \frac{y_2}{y_1}\left[\frac{(1-r_{13})\,(Y_1-y_1)+(1-r_{23})\,(Y_2-y_2)}{(r_{12}-r_{02})\,(Y_1-y_1)+(1-r_{02})\,(Y_2-y_2)}\right]. \tag{9}$$

Equating (8) and (9), we find that $y_1/y_2 = Y_1/Y_2$. Thus the ratio of the depths of the two flowing layers at the virtual control is the same as it was in the reservoir. It can be shown that there is a solution where this condition holds everywhere in the channel. This solution, found by Wood (1968), is self-similar – at every point in the channel, the ratio of the depths of the two layers is the same as their ratio at the reservoir. The continuity condition (3) requires that the ratio of velocities in the two layers is also constant everywhere. By substituting this result back into (9), the flow ratio of the self-similar solution is found to be

$$Q_r = \frac{Q_1}{Q_2} = \frac{Y_1}{Y_2}\left[\left(\frac{1-r_{01}}{1-r_{23}}\right)\left(\frac{(1-r_{13})\,Y_1+(1-r_{23})\,Y_2}{(r_{12}-r_{02})\,Y_1+(1-r_{02})\,Y_2}\right)\right]^{\frac{1}{2}}. \tag{10}$$

2.2. *The Froude-number plane*

As in Armi (1986), general solutions to the system under consideration will be presented in the Froude-number plane. The continuity equation (3) and the definition of the Froude number (4*a*) are used to find

$$y_i = \left[\frac{Q_i^2}{g_i' b^2}\right]^{\frac{1}{3}} \mathscr{F}_i^{-\frac{2}{3}}, \tag{11}$$

$$u_i = \left[\frac{Q_i g_i'}{b}\right]^{\frac{1}{3}} \mathscr{F}_i^{\frac{2}{3}}. \tag{12}$$

Non-dimensional flow rates and channel width are defined as

$$Q_i' \equiv \frac{Q_i}{[(1-r_{12})g]^{\frac{1}{2}} b_0 Y_0^{\frac{3}{2}}}, \tag{13}$$

$$b' \equiv \frac{b}{b_0}, \tag{14}$$

where b_0 a reference width and Y_0 is a reference depth, here taken to be Y_1+Y_2, the total depth of the flowing layers at the reservoir.

The preceding equations are then used to rewrite the sum of the depths of the moving layers y_1+y_2, to find

$$\left(\frac{Q_2'}{b'}\right)^{-\frac{2}{3}} = \left(\frac{Y_0}{y_1+y_2}\right)\left[\left(\frac{(1-r_{01})\,\mathscr{F}_1^2}{Q_r^2}\right)^{-\frac{1}{3}} + ((1-r_{23})\,\mathscr{F}_2^2)^{-\frac{1}{3}}\right]. \tag{15}$$

To use this result, it is also necessary to know the layer depths y_1 and y_2. The Bernoulli equations (2*a*, *b*) can be used to find the layer depths as functions of the Froude numbers:

$$y_1 = \frac{\frac{1}{2}\mathscr{F}_2^2[(1-r_{13})\,Y_1+(1-r_{23})\,Y_2]+Y_1}{D}, \tag{16a}$$

$$y_2 = \frac{\frac{1}{2}\mathscr{F}_1^2[(r_{12}-r_{02})\,Y_1+(1-r_{02})\,Y_2]+Y_2}{D}, \tag{16b}$$

where

$$D = \tfrac{1}{2}\mathscr{F}_1^2\,\tfrac{1}{2}\mathscr{F}_2^2(1-r_{12})(1-r_{03})+\tfrac{1}{2}\mathscr{F}_2^2(1-r_{13})+\tfrac{1}{2}\mathscr{F}_1^2(1-r_{02})+1. \tag{16c}$$

The energy difference between the two moving layers is found by subtracting (2*a*) from (2*b*) and in non-dimensional form is

$$\Delta E = \frac{E_2 - E_1}{\rho_2 g(1-r_{12})(Y_1+Y_2)} = \left[y_2 \left(\frac{1-r_{23}}{1-r_{03}} + (1-r_{23})\tfrac{1}{2}\mathscr{F}_2^2 \right) - y_1 \left(\frac{r_{13}-r_{03}}{1-r_{03}} + (r_{12}-r_{02})\tfrac{1}{2}\mathscr{F}_1^2 \right) \right] \frac{1}{Y_1+Y_2}. \quad (17)$$

This is a conserved quantity as long as there are no hydraulic jumps in the flow. For display in the Froude-number plane, this result can be expressed in terms of Froude numbers and the flow ratio Q_r by using (11). At the reservoir, both $\mathscr{F}_1^2$ and $\mathscr{F}_2^2$ are small so

$$\Delta E = \frac{(1-r_{23})\,Y_2 - (r_{13}-r_{03})\,Y_1}{(1-r_{03})(Y_1+Y_2)}. \quad (18)$$

This analysis can be used to present solutions in two forms. The first, used here, is similar to that used by Armi (1986). The flow ratio Q_r and layer densities are fixed and each solution curve in the Froude-number plane corresponds to different reservoir layer depths. Equations (17) and (18) are solved for $Y_2' = Y_2/Y_0$, the non-dimensional depth at the reservoir of the lower layer, and solution curves, in the form of curves of constant Y_2', are plotted. Equation (15) is used to find Q_2'/b', and using the relationship $Q' = Q_1' + Q_2' = Q_2'(1+Q_r)$, curves of constant Q'/b' are plotted. Along a solution curve, Q' is constant and the value of Q'/b' indicates the position within the contraction. In the solutions presented by Armi (1986), the Q_2'/b' curves are derived purely from the continuity equations. Here, since the total depth of the moving fluid varies, information from the energy equations, in the form of the layer depths at particular values of $\mathscr{F}_1^2$ and $\mathscr{F}_2^2$, enter into the value of Q'/b'.

It is sometimes of practical importance to find solutions with different flow ratios issuing from a known reservoir. The reservoir conditions take the form of known layer densities and values of Y_i'. Equations (17) and (18) can be solved to find Q_r in terms of the Froude numbers and reservoir conditions. For a particular set of reservoir conditions, curves of constant Q_r are solution curves, and overlying Q'/b' curves again show position within the channel along a solution curve.

3. Solutions for various layer densities

For a given flow rate and layer thickness, the Froude numbers defined by (4*a*, *b*) change when the density of the neighbouring stagnant layer changes. However, the more common definition of the layer Froude number given by (4*c*) depends only on r_{12} and so is independent of the density of the stagnant layers. Solutions sets will be plotted using this more common Froude number since this allows systems with different stagnant layer densities to be easily compared. Various solution sets will be discussed and, except where noted, in all figures the density ratio between the two flowing layers (r_{12}) will be 0.99.

The set of solutions for a flow where all four layers are separated by equal density steps and $r_{i,i+1} = 0.99$ is shown in figure 2. Lines of constant Y_2' are solution curves, and the position in the channel along a particular solution curve is given by the intersecting Q'/b' lines. The form of the solution curves is similar to those discussed by Armi (1986) and the reader is referred to that work for a detailed discussion of the presentation of solutions in the Froude-number plane. The role of the various

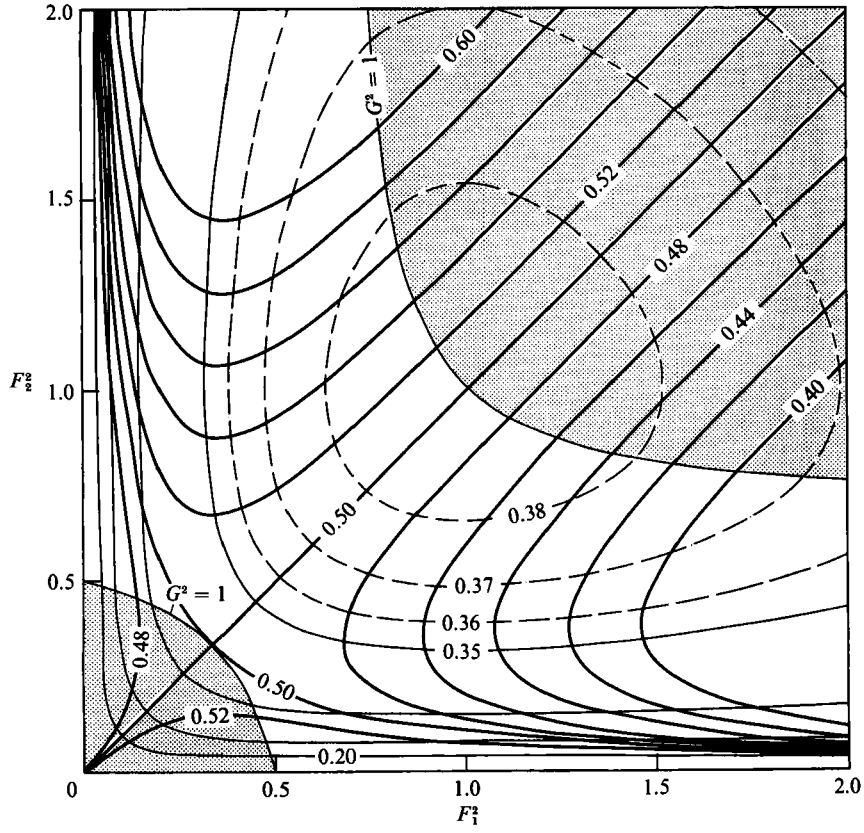

FIGURE 2. Solution curves (dark lines) and Q'/b' curves (light lines) in the Froude-number plane for $Q_r = 1$, $r_{01} = r_{12} = r_{23} = 0.99$. Each solution curve is labelled with its non-dimensional lower-layer reservoir height Y_2'. Critical flow is defined by the lines $G^2 = 1$. The Q'/b' curves are dashed for values above 0.35, where the contour interval has been reduced to 0.01.

solution curves in unidirectional flows and exchange flows has been discussed at length by Armi (1986) and by Armi & Farmer (1986). Armi also addresses the issue of internal hydraulic jumps, which must in general occur to connect a controlled flow that is supercritical in the divergent section of the channel to a subcritical downstream reservoir. We will concentrate here on the new features of the solution space that occur because we allow for variations in the total depth of moving fluid.

There are two striking differences between the solution space shown in figure 2 and those shown by Armi: the curves of constant Q'/b' are closed and have a maximum value, and there are two critical lines where $G^2 = 1$. The first critical line, at lower Froude numbers, controls the relative depths of the two moving layers. This line shows a locus of Froude numbers where the flow is critical with respect to the higher internal wave mode. At the second critical line, the flow is critical with respect to the lower internal mode, and the total depth and volume flux of the moving fluid are controlled. In the following discussion, a flow that is supercritical with respect to only the higher mode will be referred to as internally supercritical while a flow that is supercritical with respect to both modes will be referred to as fully supercritical. Armi (1986) assumes that the total depth of the two layers is constant, which filters out the lower mode and removes the control of the total volume flux associated with the second critical line.

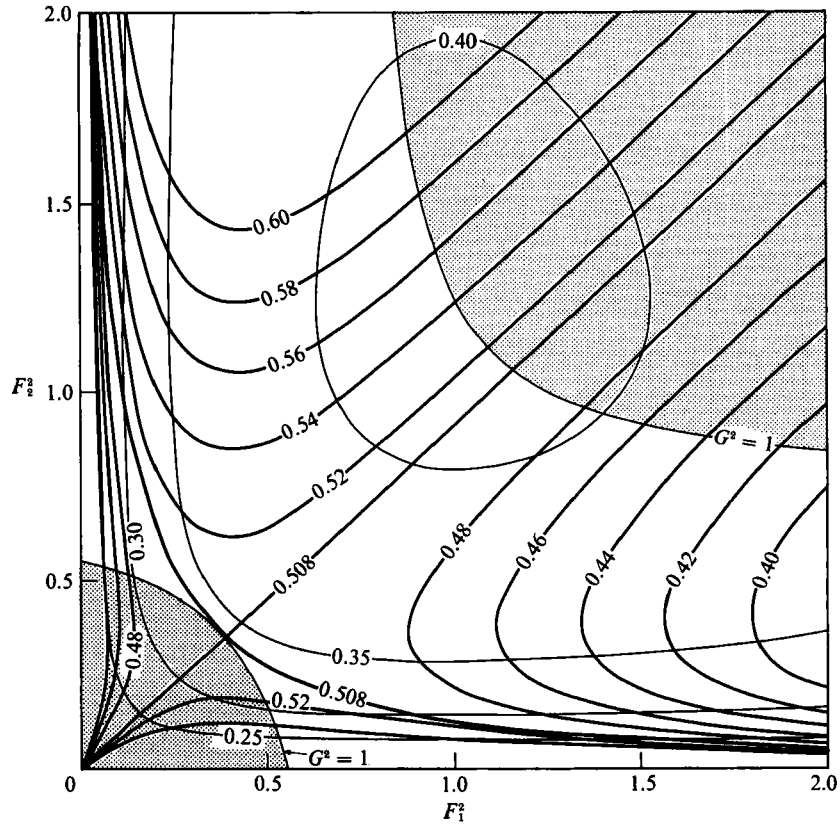

FIGURE 3. As figure 2 but for $r_{01} = r_{12} = r_{23} = 0.8$.

The solution space in figure 2 is also slightly asymmetric about the line $F_1^2 = F_2^2$, an effect due to not using the Boussinesq approximation. This effect is small since the density ratios $r_{i,i+1}$ are all close to 1. It is illustrated more dramatically in figure 3, which shows the solution space for the case $r_{i,i+1} = 0.8$. There is a marked asymmetry in the solution space due to non-Boussinesq effects, but the overall structure of the solution space is unchanged. The following discussion of the features of the solution space applies equally well to either figure.

The self-similar solution curve is the straight line coming from the origin. It is the only solution curve that passes through both critical lines. The point at which it passes through the first (low Froude number) critical line is the virtual control. It passes through the second critical line at the narrowest section and so the value of Q'/b' is a maximum there. It is the only solution that originates at a stagnant reservoir, where both F_1^2 and F_2^2 are zero, and passes through the second (high Froude number) critical curve.

Another important solution curve is the one that crosses the self-similar solution, the maximal exchange solution found by Wood (1970) and discussed at length by Armi & Farmer (1986). It connects two reservoirs, one where layer 1 is moving at high Froude numbers and the other where layer 2 is moving at high Froude numbers. The self-similar solution and the maximal exchange solution are the only two solution curves that intersect. Every critical point on a solution curve is at the narrowest section except the virtual control point, where the self-similar and maximal exchange solutions intersect. This can be seen by noticing that, except in

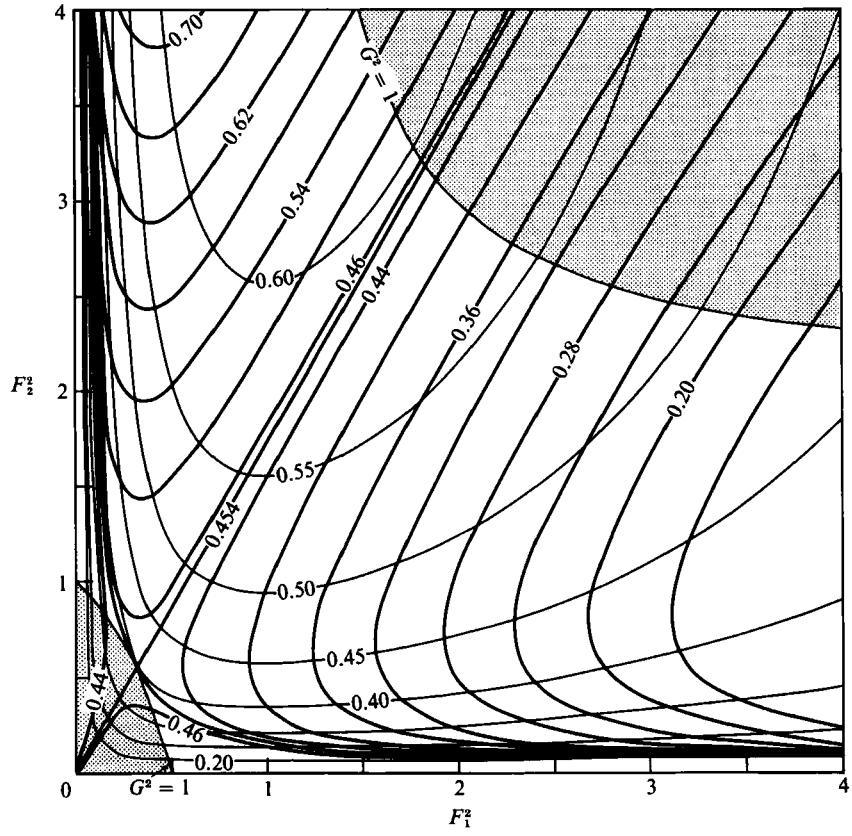

FIGURE 4. Solution curves (dark lines) and Q'/b' curves (light lines) in the Froude-number plane for two layers flowing beneath a stagnant layer ($Q_r = 1$, $r_{01} = r_{12} = 0.99$ and $r_{23} = 0$). Each solution curve is labelled with its non-dimensional lower-layer reservoir height Y_2'. Critical flow is defined by the lines $G^2 = 1$.

this one case, every solution curve reaches a maximum value of Q'/b', and hence a minimum value of b', when it passes through a critical line.

Other flow geometries are obtained by removing one of the stagnant layers. Lai & Wood (1975) studied the flow of two layers beneath a stagnant layer, obtained here by setting $r_{i3} = 0$ and referred to as a $2\frac{1}{2}$-layer system. Solution curves for this system with $r_{01} = 0.99$ and $r_{12} = 0.99$ are shown in figure 4. Solutions for the flow of two layers over a stagnant layer, obtained by setting $r_{0j} = 0$, are essentially identical to those shown in figure 4 but with the layer indices exchanged; there is a slight asymmetry due to non-Boussinesq effects, but it is not significant at the density ratios used in figure 4. The basic features of these solution sets are the same as those discussed above. Figure 4 of Lai & Wood (1975) shows a set of solution curves analogous to those shown here in figure 4, although Lai & Wood do not use a Froude-number parameterization. They dismissed as unphysical the non-self-similar solution curves that lie above the lower-Froude-number critical line. In two-layer systems, the role of these solution curves in the divergent section of the contraction was discussed by Armi (1986), and these solutions play an identical role in all the systems considered here.

The behaviour of the $2\frac{1}{2}$-layer system will be explored further by changing the density of the stagnant layer, which changes the value of r_{01}. Figure 5 shows the

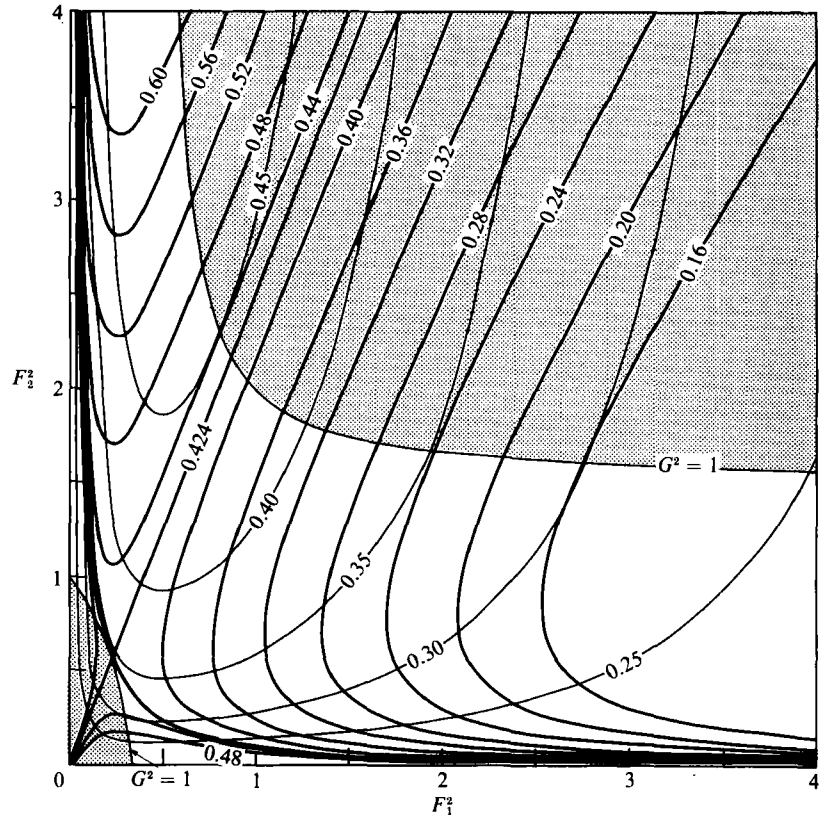

FIGURE 5. As figure 4 but for $r_{01} = 0.995$, $r_{12} = 0.99$ and $r_{23} = 0$.

solution curves for $r_{01} = 0.995$; the density step between the moving and stagnant layers is half the size of the density step between the two moving layers. The features seen in figure 4 are reproduced in this figure, but they occur at lower Froude numbers, and the angle of the critical flow line relative to the horizontal axis is greater. Thus the ratio F_1^2/F_2^2 of the self-similar solution is smaller than in figure 4 and so the lower layer is accelerated more and the upper layer less than in the self-similar solution of figure 4. Apart from this skewing of the solution curves, the behaviour of the solution curves relative to the critical lines is identical to that described above. The critical lines are closer together and have both moved closer to the origin. The Q'/b' curves show that critical flows occur at lower flow rates than in figure 4.

Figure 6 shows the solution curves for $r_{01} = 0.98$ – the density step between the moving and stagnant layers is twice the size of the density step between the two moving layers. In order for the second critical line to be plotted, the size of the Froude-number space is larger than that used in figures 4 and 5. Again, the features described earlier are reproduced, but now they occur at higher Froude numbers. Similarly, the rotation of the self-similar flow line from its position in figure 4 is in the opposite direction to that in figure 5, and the values of Q'/b' at critical points are greater than in figure 4. The curvature of the critical lines is less than in figure 4 and if the upper density step is taken to its extreme value, so that $r_{01} = 0$, the first critical line flattens out and the second critical line moves to very large Froude numbers. The first critical line becomes a straight line when the approximation $r_{12} = 1$ is made and results of Armi (1986) are recovered.

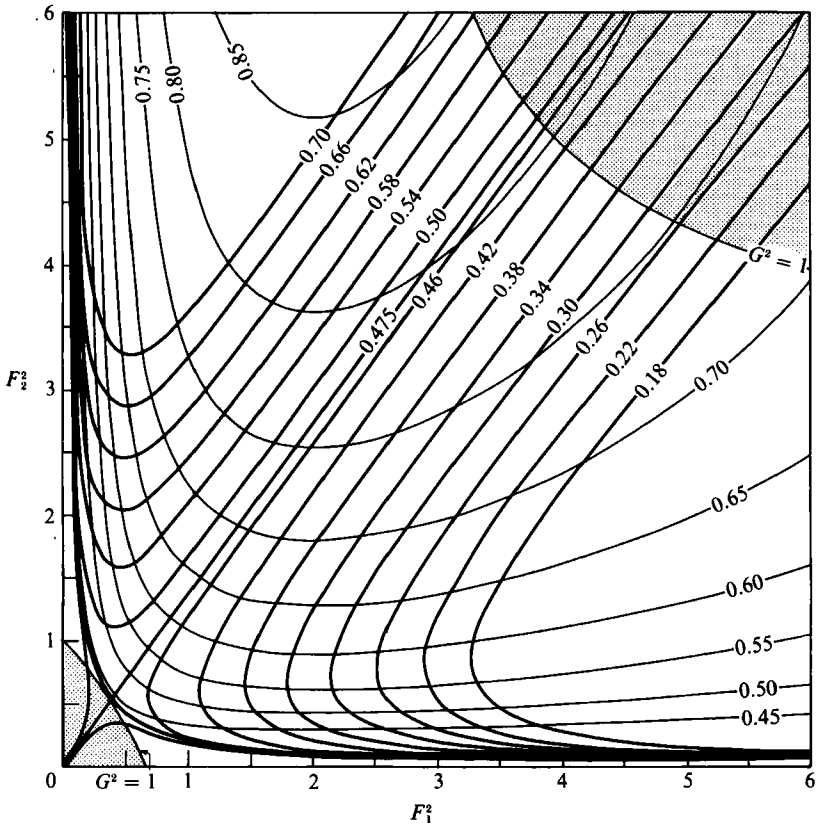

FIGURE 6. As figure 4 but for $r_{01} = 0.98$, $r_{12} = 0.99$ and $r_{23} = 0$.

4. Plunging flows

The existence of two-layer plunging flows can be anticipated by considering the following situation. Two layers are flowing beneath a stagnant layer, the flow is self-similar and there are two controls: a virtual control within the contraction and a control at the narrowest section. The flow rate and reservoir conditions are such that at the reservoir, and only there, the thickness of the stagnant layer is zero. A side view of this flow is illustrated in figure 7, labelled with lower-layer reservoir depth $Y_2 = 0.454$. The dashed vertical line marks the position of the narrowest section. The total volume flux of each solution discussed in this section will be normalized relative to the volume flux of this flow, the maximal self-similar flow, and will be referred to as Q_{REL}. When the total flow rate is increased, the $2\frac{1}{2}$-layer self-similar flow can no longer occur. A two-layer flow leaves the reservoir but at some point in the contraction, the interface between the moving fluid and the stagnant top layer intersects the free surface, and downstream of that point, there is a $2\frac{1}{2}$-layer flow. The maximal self-similar flow and two plunging flows are sketched in figure 7, where the plunge point is labelled S. The solution curves shown in this figure are for the case $r_{01} = 0.99$, $r_{12} = 0.99$ and will be discussed later in this section.

The box flows discussed by Armi & Farmer (1986) are single-layer flows that have a transition within the contraction from single-layer dynamics to $1\frac{1}{2}$-layer dynamics. In the flows considered here, there is a transition within the contraction from two-layer to $2\frac{1}{2}$-layer dynamics. We will study four flow regimes, differentiated by the positions of the two controls relative to the positions of the transition point and the

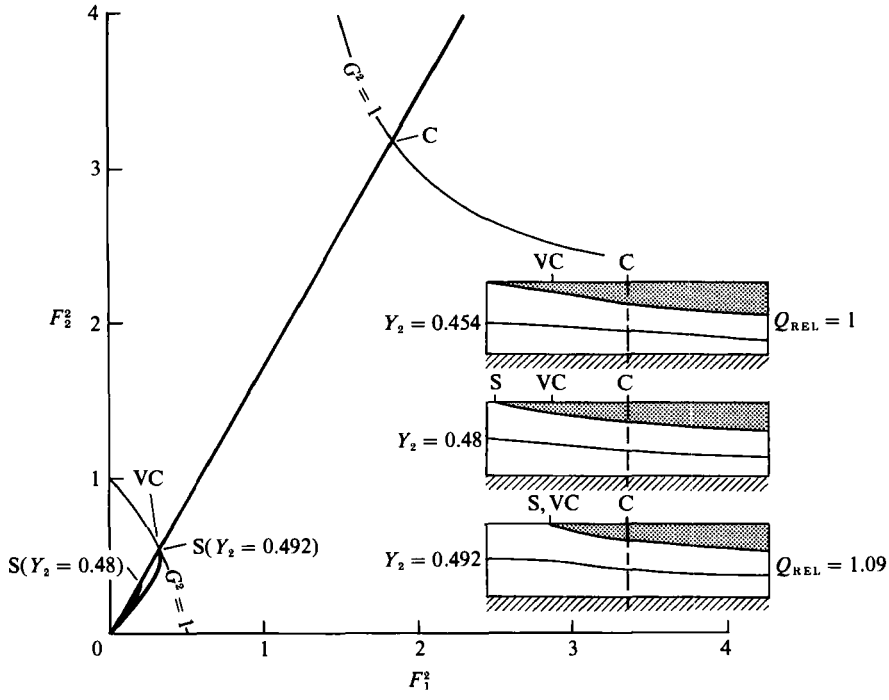

FIGURE 7. Solution curves and schematic diagrams of regime (i) plunging flows: S, transition point; VC, virtual control; C, control.

narrowest section. Both the virtual control and the narrowest section can occur in either the two-layer or $2\frac{1}{2}$-layer portion of the flow.

Other flow geometries give rise to similar plunging flow problems. When two layers flowing above a stagnant layer and the depth of the stagnant layer becomes zero within the contraction, the problem is simply an inverted version of the flow outlined above. Two layers can also flow between two stagnant layers and the depth of one or both of the stagnant layers can become zero within the contraction. These flows are not fundamentally different from the case outlined above, and so only that situation will be considered in detail.

A set of solutions will be presented for the case $Q_r = 1$. Solution curves will again be shown in a Froude-number plane, and in all cases the axes will be labelled with values of F_i^2, the Froude number defined in (4*c*) and used in earlier figures. The $2\frac{1}{2}$-layer solutions are matched to the two-layer solutions by requiring that the layers in each region have the same depths at the transition point. The four regimes are as follows:

(i) Three solution curves for this regime are shown in figure 7, along with schematic diagrams showing the side view of a channel for each of the solution curves. Various points of significance are marked: C shows the control at the narrowest section; VC shows the virtual control; S shows the transition from two-layer flow to $2\frac{1}{2}$-layer flow. When the transition occurs, the $2\frac{1}{2}$-layer regime is subcritical and so the only possible $2\frac{1}{2}$-layer solution is the self-similar solution. The flow in the two-layer portion matches this solution at the transition. The three schematic diagrams show that as the flow rate is increased, the transition point moves downstream until it coincides with the virtual control. The virtual control is always at the same position because the same self-similar $2\frac{1}{2}$-layer flow occurs in all

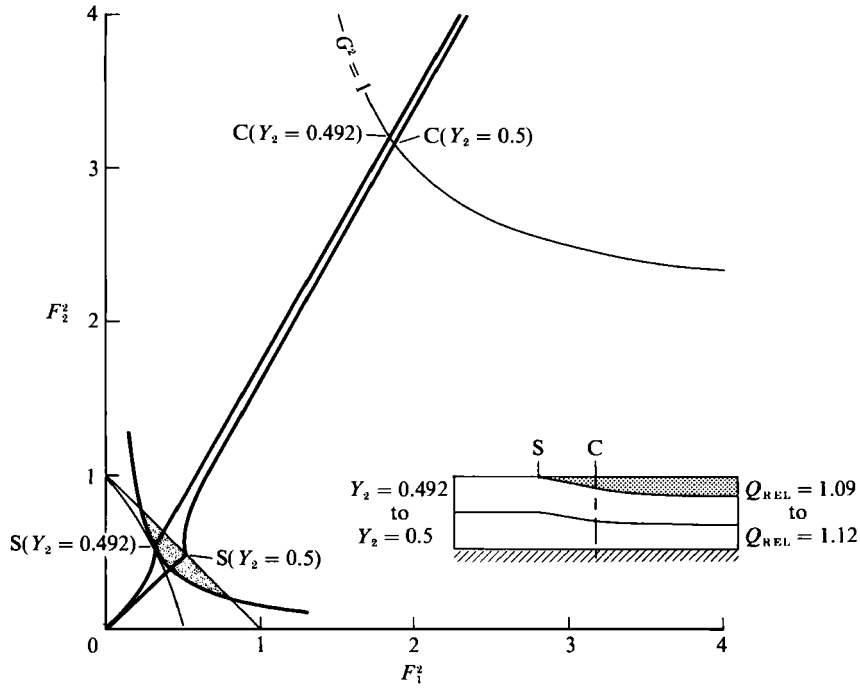

FIGURE 8. Solution curves and schematic diagram of regime (ii) plunging flows: S, transition point; C, control.

flows in this regime. The schematic diagrams are labelled with the lower-layer reservoir depth Y_2' and with Q_{REL}. When $Q_{\mathrm{REL}} = 1$, $Y_2' = 0.454$ and at the highest flow rate in this regime, $Q_{\mathrm{REL}} = 1.09$ and $Y_2' = 0.492$.

(ii) When the transition occurs in this regime, the flow in the two-layer portion is subcritical and flow in the $2\frac{1}{2}$-layer portion is internally supercritical. Like a virtual control, the transition point marks a transition between subcritical flow and internally supercritical flow. Unlike a virtual control, this point is also the transition from two-layer dynamics to $2\frac{1}{2}$-layer dynamics. The situation is unusual in that there is a range of possible flows.

The area in the Froude-number plane that delineates possible transition points is shown in figure 8, which also shows two solution curves and a schematic diagram of a flow in this regime. The area of possible transitions is defined by two curves. Since the two-layer flow must be subcritical, the area is bounded on the upper side, at higher Froude numbers, by the two-layer critical line. Since the $2\frac{1}{2}$-layer portion of the flow must be internally supercritical and in the convergent part of the channel, the area is bounded on the lower side, by the solution curve for the $2\frac{1}{2}$-layer system that is the maximal exchange solution, or the critical curve for the $2\frac{1}{2}$-layer system where the maximal exchange flow is subcritical. Within this area, multiple solutions having the same total flow rate are possible. Each possible solution matches to a different two-layer solution and so comes from a different reservoir condition.

Referring to the solution curves in figure 8, C shows the control at the narrowest section and S shows the transition from two-layer flow to $2\frac{1}{2}$-layer flow. At the transition point S, the flow changes from subcritical to internally supercritical but since for a particular flow rate there is a range of possible reservoir conditions, the flow is controlled by the reservoir conditions rather than at the transition point. At the highest flow rate in this regime, the two-layer flow is just critical at the transition

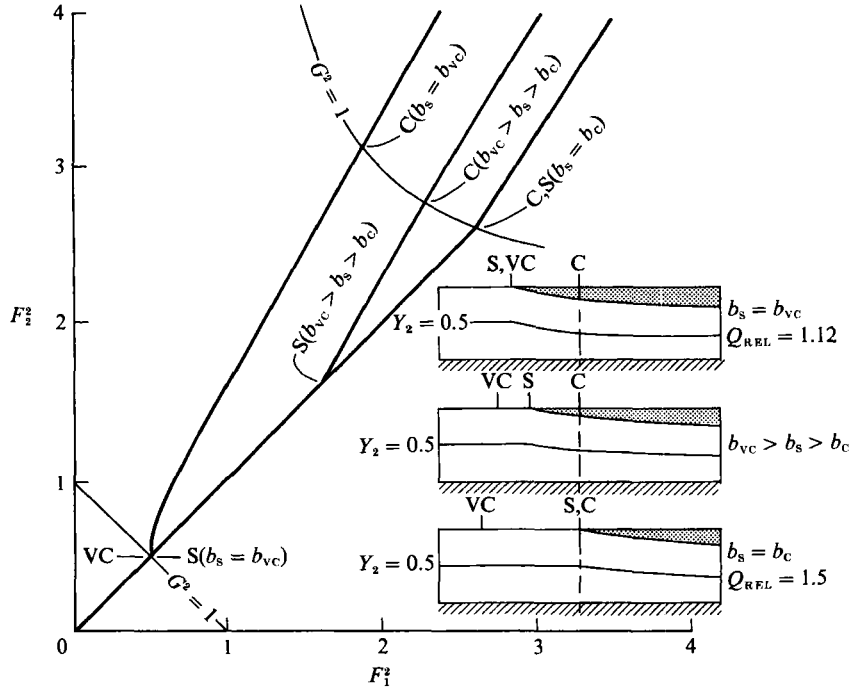

FIGURE 9. Solution curves and schematic diagrams of regime (iii) plunging flows: S, transition point; VC, virtual control; C, control.

and so the layer depths in the reservoir are equal ($Y_2' = 0.5$). This reservoir condition holds for both subsequent regimes.

The transition between two-layer dynamics and $2\frac{1}{2}$-layer dynamics is such that there is a range of reservoir conditions possible for a single flow rate. A similar behaviour was found by Bryant & Wood (1976) when studying two layers flowing in a channel that narrowed and had a down-sloping roof. As the total flow rate increased, there was a transition from a flow with a virtual control in a region governed by two-layer dynamics to a flow with a virtual control in a region governed by $2\frac{1}{2}$-layer dynamics. They found conditions for which there was an under-constrained 'overlap' region analogous to the regime (ii) flows discussed here. There was also an over-determined, unsteady region that does not occur in the system studied here.

The range of solutions spans a small range of reservoir conditions and flow rates so the anticipated multiple solutions would be difficult or impossible to observe in laboratory experiments. The fact that there is a small range of solutions rather than a completely controlled flow is unlikely to be of practical importance.

(iii) Figure 9 shows solution curves and schematic diagrams for three flows in this regime. The two-layer flow passes through a virtual control and so the solution in the two-layer region is the self-similar solution already discussed by Armi (1986). The transition (S) is to a $2\frac{1}{2}$-layer flow that is internally supercritical and becomes fully supercritical downstream of the narrowest section (C). Since we are discussing the case $Q_r = 1$, all the flows in this regime come from a reservoir with equal depth layers. At the start of this regime, the two layers have different depths and speeds at the narrowest section. As the flow rate increases, the transition point (S) moves towards the control at the narrowest section (C), and there is a smaller difference in layer

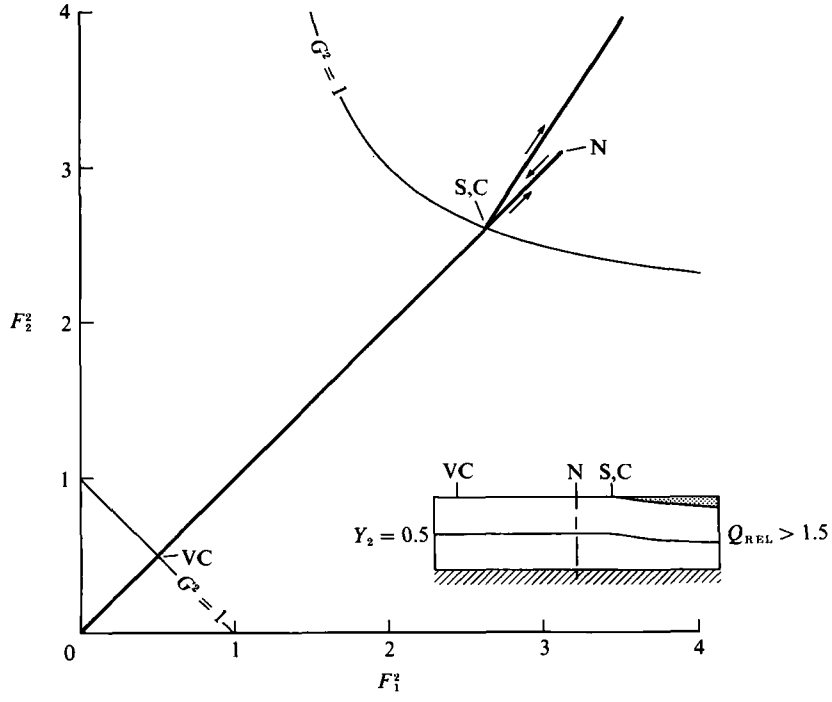

FIGURE 10. Solution curves and schematic diagram of regime (iv) plunging flows: S, transition point; VC, virtual control; N, narrowest section; C, control.

speed and depth at this point. At the highest flow rate in this regime, the two-layer self-similar solution holds all the way to the narrowest section. The transition point and control both occur at this section, and the two layers have equal speeds and depths.

(iv) Figure 10 shows a solution curve and schematic diagram for a flow in this regime. The two-layer flow passes through a virtual control and then passes through the narrowest section (N) but is not controlled there. The flow remains a two-layer flow and as the channel diverges, the flow returns toward the reservoir conditions along the same solution curve. At the point at which the corresponding $2\frac{1}{2}$-layer solution is just critical, the flow switches to that flow regime and continues down the channel as a fully supercritical $2\frac{1}{2}$-layer flow. Like highest volume flow in regime (iii), this solution is critical at the transition and so this point is also a control.

5. Experiments

The solutions discussed in §§3 and 4 have been explored in a series of laboratory experiments. The experimental facility is shown in figure 11. A narrow channel is connected to a large reservoir (123 × 246 cm), the channel and reservoir have flat bottoms and are approximately 22 cm deep. The channel is 10.3 cm wide, narrowing to 2.2 cm in the contraction; the total length of the convergent–divergent section is 61 cm. In the narrowest part of the contraction, the streamwise variation of the channel width was quite small, changing by ~ 0.5 mm/cm in the 4 cm on either side of the narrowest section.

The flow of two layers beneath a stagnant layer and two-layer plunging flows were realized by filling the reservoir with fresh water and pumping two layers of denser

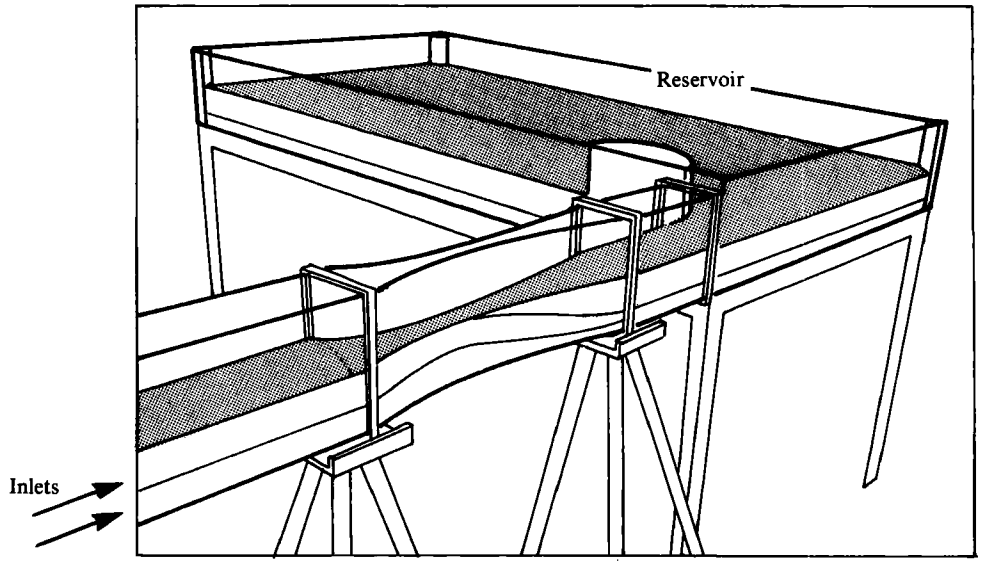

FIGURE 11. Sketch of the experimental facility.

salt water into the reservoir through the contraction while withdrawing water from the reservoir to maintain constant depth in the channel and reservoir. Flow in the two moving layers was controlled by gear pumps whose flow rates were continuously variable. At the inlet, the layers were separated by splitter plates. Each inlet contained a region of high pressure loss consisting of open-cell foam, stainless-steel wool and plastic honeycomb. The large pressure drop resulted in a uniform flow in each layer. The upper moving layer was dyed, which allowed visualization of the density interfaces.

Three set of experiments will be discussed. In the first, flows with only one control in the contraction were created by placing a weir in the channel far downstream from the contraction, at the connection to the reservoir. The weir controlled the total depth of the two moving layers, while the relative thickness of the layers was controlled by the contraction. In the second set of experiments, the downstream weir was removed. The total depth was then controlled at the narrowest section, and there was a virtual control in the convergent section of the channel that controlled the relative thickness of the two layers. The only flow of this type is Wood's self-similar solution. In both these sets of experiments, the channel and reservoir were filled to a depth of approximately 18 cm and the overlying stagnant layer was quite thick. Both these sets of experiments were carried out with two different sets of layer densities to illustrate the effects of changing relative layer densities discussed in §3. Finally, the plunging flows of §4 were studied. In this set of experiments, in order to match the upstream flow to the inlet diffuser and to perform experiments at flow rates that the pumps could create, the reservoir and channel were filled to a depth of approximately 10.5 cm.

The most important predictions of the theory are the conditions at the narrowest section, where the flow is typically controlled, so we measured the layer Froude numbers at the narrowest section. In all the experiments, the layer thicknesses were measured to ± 0.5 mm and the density difference between adjacent layers was measured to $\pm 10^{-4}$ g/cm^3. These errors give an error in the measured Froude number, depending on the layer thickness, of 5–10%. Velocities in each layer were

assumed constant. This was tested by dropping potassium permanganate crystals into the flowing layers. The assumption is reasonable, although there were noticeable boundary layers both at the walls of the channel and between layers moving at markedly different speeds. A consequence of the sidewall boundary layers is that the effective width of the channel is different from the measured channel width and since the sidewall boundary layers grow with downstream position, the effective position of the narrowest section is displaced downstream of the geometric narrowest section. Another source of error is that although the channel width changed slowly in the vicinity of the narrowest section, the slopes of the interfaces in that area were sometimes not negligible and so one must expect some deviations from the hydrostatic and one-dimensional assumptions that the hydraulic theory relies upon.

5.1. *Flows with one control*

The total depth of the flows discussed here was controlled by a 7 cm high weir located at the entrance to the reservoir, far downstream of the contraction. The resulting flows are analogous to those discussed by Armi (1986), except that here the total depth of the two moving layers changes considerably as the flow passes through the contraction. The theory of §3 shows that for any flow rate at which flow at the narrowest section is critical with respect to the higher mode, there are two controlled solutions: one accelerates the upper layer in the divergent section and the other accelerates the lower layer. Armi (1986) demonstrated both solutions by using both a conventional weir and an inverted weir to control the free-surface level. Here, we have only used a conventional weir, and so only created the solution in which the upper layer is accelerated in the divergent section. Since we are studying flows beneath a stagnant layer, this situation is the more physically relevant one.

Conditions at the narrowest section for flows with one control have been plotted in the Froude-number plane. Figure 12(*a*) shows these data for $r_{01} = 0.9936$, $r_{12} = 0.9953$, and photographs of two of the flows are shown in figures 12(*b*) and 12(*c*). The theoretical Q'/b' curves, critical flow curve, self-similar solution curve and solution curves for the flows in figures 12(*b*) and 12(*c*) are also shown in the Froude-number plane. Each data point is labelled with the value of Q'/b' at the narrowest section. The flows are controlled at the narrowest section or have a virtual control in the convergent part of the channel and are internally supercritical at the narrowest section. At the narrowest section, we would expect to see in the first case that the data points fall on the low-Froude-number critical line and in the second case that the data points lie on the self-similar flow solution curve beyond the first critical flow line. The deviations from these theoretical predictions, for reasons outlined above, are similar to those seen in the two-layer experiments reported by Armi (1986).

Figure 12(*b*) is an example of a flow with a highest mode control at the narrowest section. The flow comes from upstream conditions (the left-hand side of the picture) where both Froude numbers are small. As the channel converges, both layers accelerate and at the narrowest section the flow is critical with respect to the slower internal wave mode. In the divergent section of the channel, the flow is supercritical with respect to this mode while the upper layer thins and accelerates, and the lower layer thickens and decelerates.

As the total flow rate is increased, eventually the volume flux is high enough so that the highest mode cannot be controlled at the narrowest section. The self-similar solution flows into the contraction and the slower mode is controlled at a virtual control upstream of the narrowest section, but the flow rate is not high enough for the faster mode to be controlled at the narrowest section. Lai & Wood (1975)

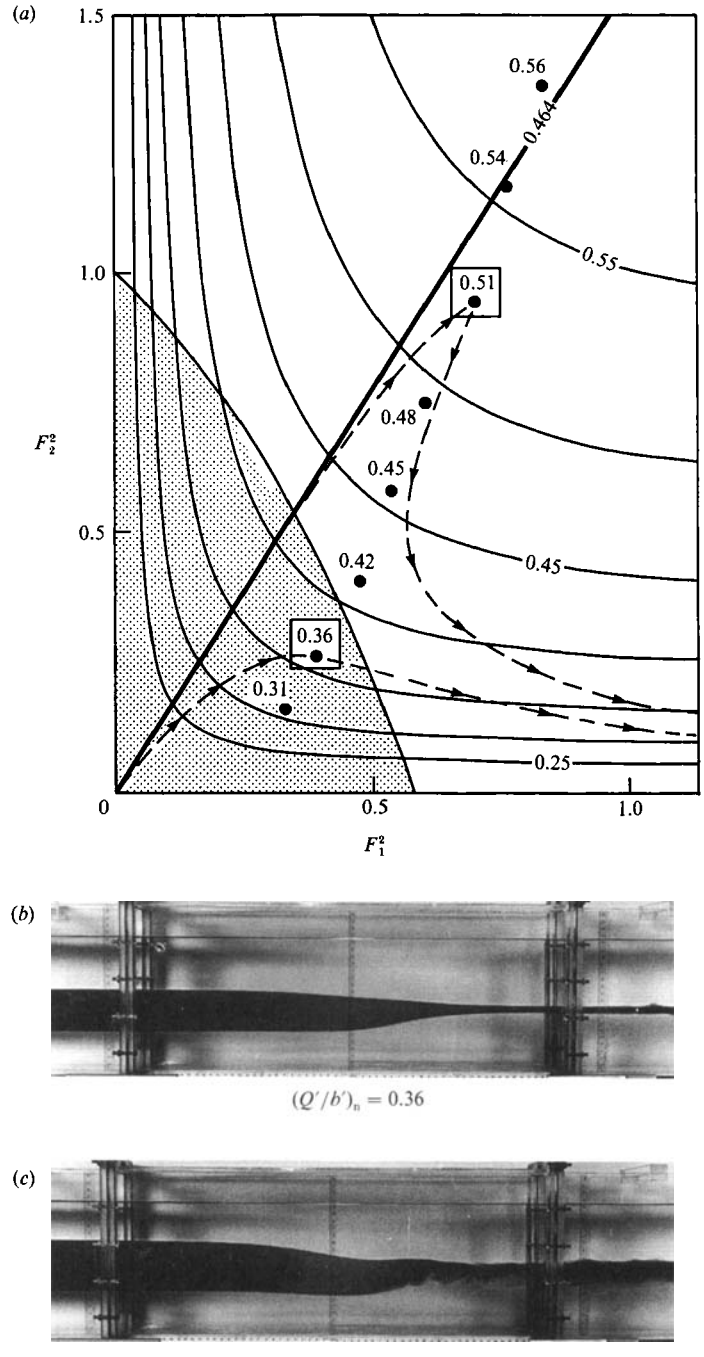

FIGURE 12. (*a*) Experimental values of the internal Froude numbers at the narrowest point in the contraction for flows with $r_{01} = 0.9936$, $r_{12} = 0.9953$ and $Q_r = 1$. Each point is labelled with the experimental value of Q'/b'. The theoretical values of Q'/b' are shown, along with the critical flow lines and the self-similar solution curve. The dashed lines show the solution paths for the flows shown in (*b*) and (*c*), where flow is from left to right and the vertical ruler marks the narrowest section. (*b*) Flow through the contraction with $Q'/b' = 0.36$. (*c*) Flow through the contraction with $Q'/b' = 0.51$.

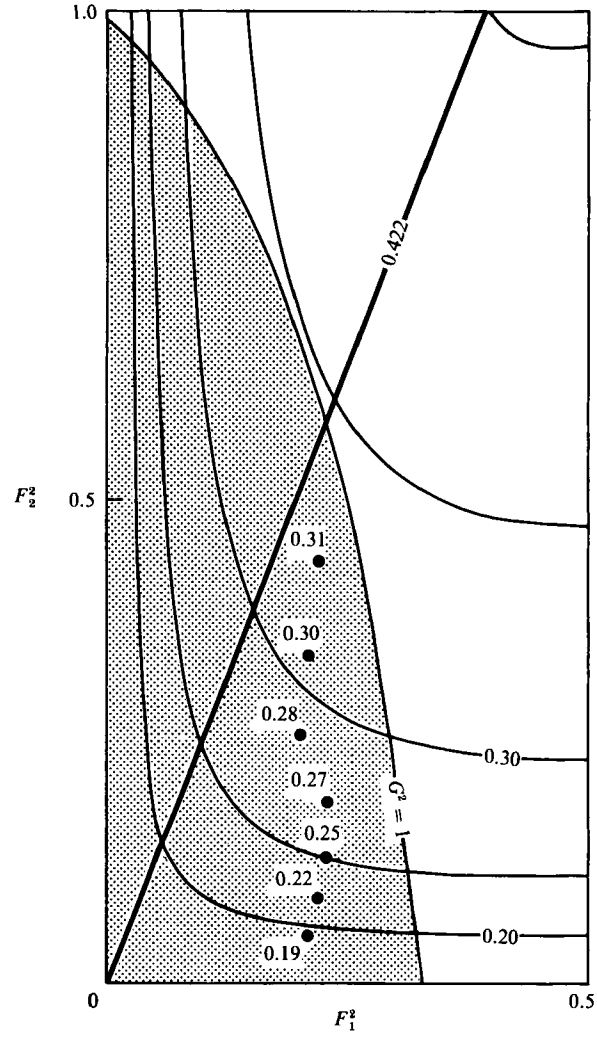

FIGURE 13. Experimental values of the internal Froude numbers at the narrowest point in the contraction for flows with $r_{01} = 0.9961$, $r_{12} = 0.9919$ and $Q_r = 1$. Each point is labelled with the experimental value of Q'/b'. The theoretical values of Q'/b' are shown, along with the critical flow lines and the self-similar solution curve.

considered the hydraulic theory for such a flow in a $2\frac{1}{2}$-layer system and hypothesized that the flow would be symmetric about the narrowest section. Armi (1986) found an asymmetric flow in the analogous flow in a two-layer system. Figure 12(*c*) shows this flow in the $2\frac{1}{2}$-layer system. The flow is similar to the two-layer flow found by Armi (1986). It is self-similar in the convergent section of the channel and both layers thin as the channel narrows. The flow passes through a virtual control and is supercritical with respect to the slower internal mode at the narrowest section. In the divergent section, instead of returning along the same solution branch, the flow is perturbed slightly from the self-similar branch, remains supercritical and accelerates the upper layer. The shear between the stagnant fluid and this accelerated layer, and between the two moving layers, resulted in an unstable flow in the divergent section.

Figure 13 shows data for $r_{01} = 0.9961$, $r_{12} = 0.9919$ in a manner equivalent to that of figure 12(*a*). The data points show measured Froude number at the narrowest

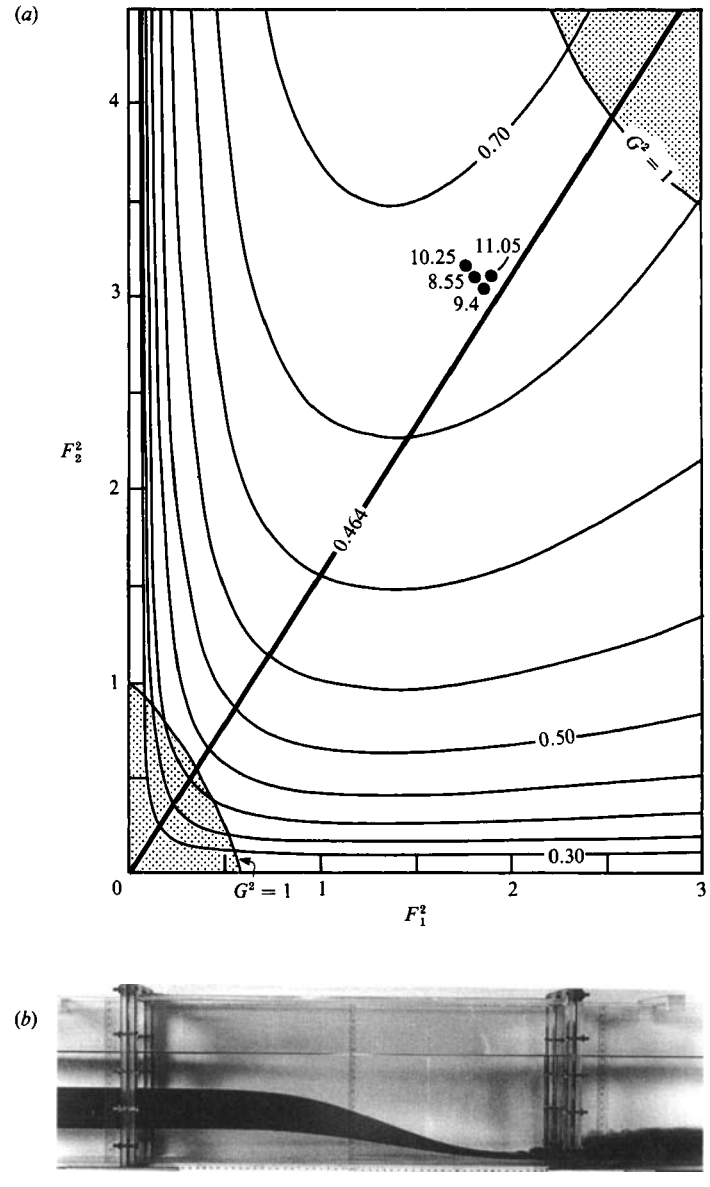

FIGURE 14. (*a*) Experimental values of the internal Froude numbers at the narrowest point in the contraction for self-similar flows with $r_{01} = 0.9936$, $r_{12} = 0.9953$ and $Q_r = 1$. Each point is labelled with the total depth in cm at the inlet of the moving layers. The theoretical values of Q'/b' are shown, along with the critical flow lines and the self-similar solution curve. (*b*) Self-similar flow through the contraction. Flow is from left to right and the vertical ruler marks the narrowest section.

section for a range of flow rates so we again expect the data points to lie along the critical curve and, at higher flow rates, to be on the self-similar solution line. The form of the critical curve and the values of Q'/b' of the experimental flows are quite different from the situation shown in figure 12(*a*). However, the systematic deviations from the theoretical predictions are similar to those seen in figure 12(*a*) and by Armi (1986).

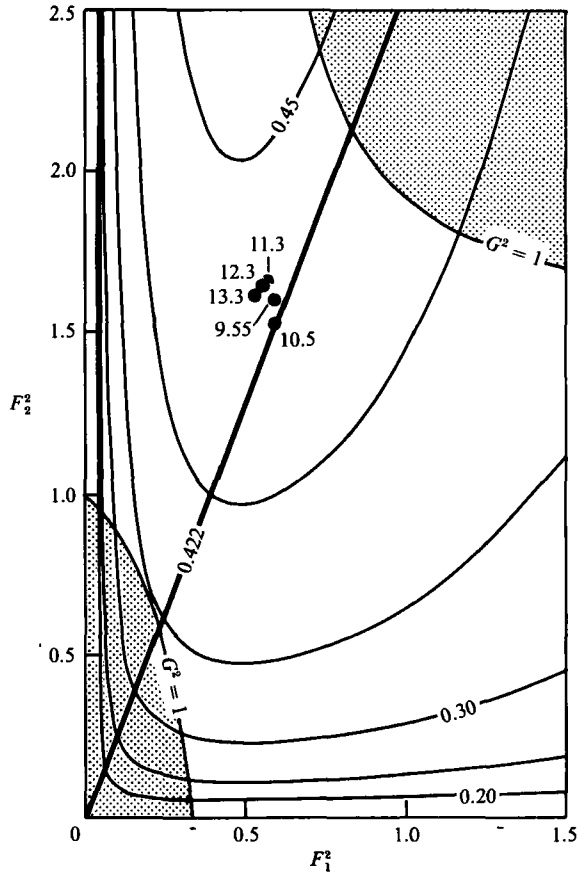

FIGURE 15. Experimental values of the internal Froude numbers at the narrowest point in the contraction for self-similar flows with $r_{01} = 0.9961$, $r_{12} = 0.9919$ and $Q_r = 1$. Each point is labelled with the total depth in cm at the inlet of the moving layers. The theoretical values of Q'/b' are shown, along with the critical flow lines and the self-similar solution curve.

5.2. *Self-similar flows*

When the downstream weir is removed, there is only one point of constriction in the experimental apparatus, and the resulting controlled flow is Wood's self-similar solution. The conditions at the narrowest section for the self-similar flows with $r_{01} = 0.9936$, $r_{12} = 0.9953$ are plotted in the Froude-number plane in figure 14(*a*), and a photograph of the flow is shown in figure 14(*b*). The theoretical Q'/b' curves, critical flow curves and the self-similar solution curve are also shown in the Froude-number plane. The flows respond to changes in volume flux by changing the total depth of the moving layers and theoretically all self-similar flows for a given set of layer densities have the same value of Q'/b' at the narrowest section. These flows are therefore labelled with the total volume flux. Theoretically, at the narrowest section, all these flows should be at the point in the Froude-number plane where the self-similar solution line crosses the outer critical curve and the flow should be critical with respect to the faster wave mode. While all the data points lie close to the self-similar solution line, the measured Froude numbers are consistently smaller than the theoretically predicted values, a result that is consistent with the idea that the effective narrowest section is displaced downstream of the geometric narrowest section by the sidewall boundary layers.

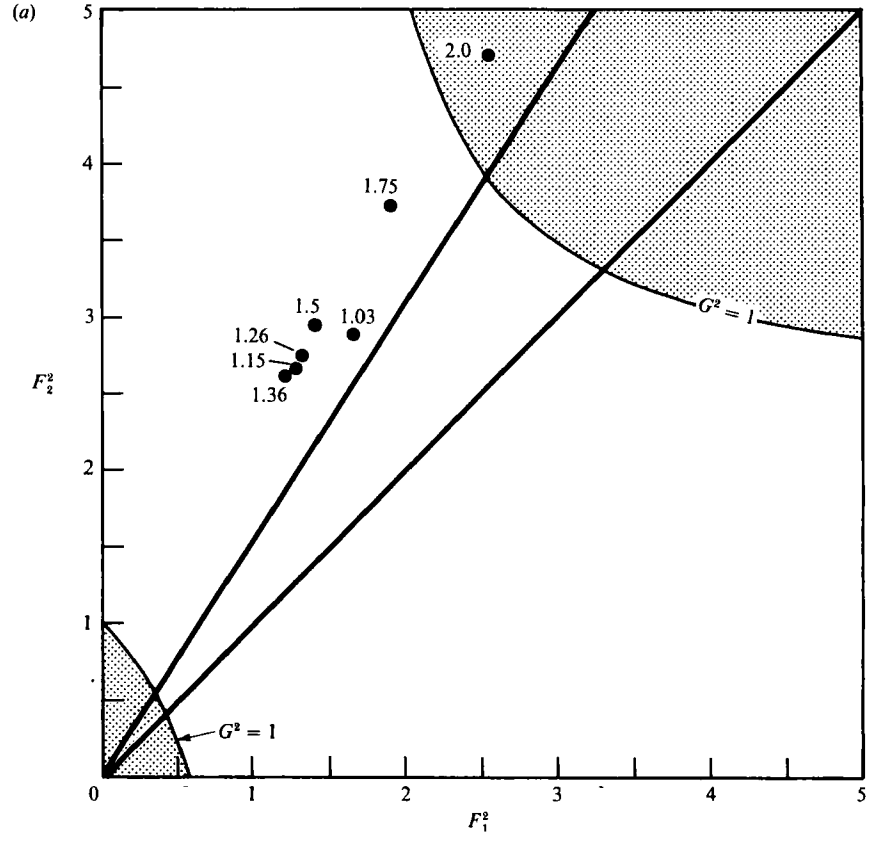

(b)

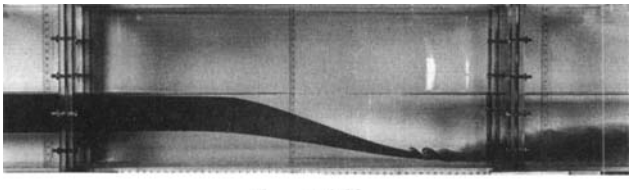

$Q_{\mathrm{REL}} = 1.03$

(c)

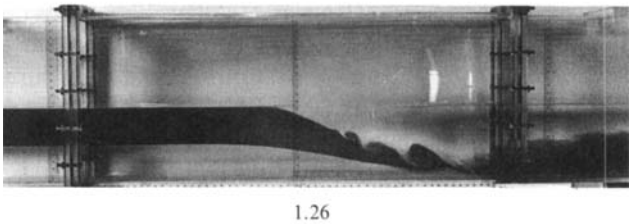

1.26

(d)

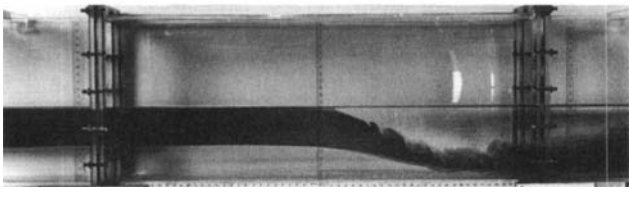

1.75

FIGURE 16. For caption see facing page.

Referring to figure 14(*b*), the ratio of the layer depths (y_1/y_2) is constant throughout the channel. The total depth of the moving layers is controlled at the narrowest section and there is a virtual control upstream of the narrowest section that controls the relative depth of the two layers. This solution is the only fully controlled solution so when the total volume flux is changed, the flow responds by changing its total depth but keeping the same self-similar form. Despite the slow streamwise variation in channel width, the slope of the layer interfaces close to the narrowest section is quite large. In the divergent part of the channel, the moving layers are accelerated and eventually the flow becomes unstable owing to the large shear at the top of the moving layers.

Froude-number values at the narrowest section for self-similar flows with the density profile $r_{01} = 0.9961$, $r_{12} = 0.9919$ are shown in figure 15. As in the data shown in figure 14, we expect these data points to fall at the point in the Froude-number plane where the self-similar solution line crosses the outer critical curve. We again see that the data points are close to the self-similar solution line but that the observed Froude numbers at the narrowest section are significantly smaller than the theoretically predicted values.

5.3. *Plunging flows*

The sequence of plunging flows described in §4 was studied by establishing a self-similar flow and then increasing the total flow rate while keeping the flow ratio constant. Figure 16(*a*) shows conditions at the narrowest section for the plunging flows with $r_{01} = 0.9936$, $r_{12} = 0.9953$. As in the theoretical solutions, figures 7–10 discussed in §4, each experiment is labelled with the total volume flux normalized with the volume flux of the theoretical maximum self-similar flow. Figure 16(*a*) also shows the critical flow curves and the self-similar solution curves for the two-layer flow (the less steeply sloping straight line) and the self-similar solution curve for the $2\frac{1}{2}$-layer flow (the more steeply sloping straight line). When the flow rate is slightly greater than the maximum self-similar flow, the plunging flow has its plunge point upstream of the virtual control and the theory predicts that the $2\frac{1}{2}$-layer portion of the flow is self-similar. A flow of this type, corresponding to regime (i) of §4 (figure 7), is shown in figure 16(*b*).

As the flow rate is increased, the plunge point moves downstream into the contraction. A regime (iii) (figure 9) plunging flow, in which the plunge point has moved downstream of the virtual control, is shown in figure 16(*c*). In this flow, the plunge line is angled quite sharply across the channel, a ubiquitous feature of plunging flows at higher flow rates that was not anticipated by the simple hydraulic theory. Downstream of the plunge point, the interface between the moving and stagnant layers is unstable. The instability mixes some of the stagnant fluid into the upper moving layer but the lower moving layer flows unmixed into the reservoir.

A regime (iv) (figure 10) plunging flow is shown in figure 16(*d*). At this higher flow rate, there are higher shears at the interface between moving and stagnant fluid. The onset of instability has moved upstream towards the plunge point so far that the instability interacts with the plunge point. It was observed that the position of the

FIGURE 16. (*a*) Experimental values of the internal Froude numbers at the narrowest point in the contraction for plunging flows with $r_{01} = 0.9936$, $r_{12} = 0.9953$ and $Q_r = 1$. Each point is labelled with the total volume flux relative to the flux in the maximal self-similar flow. The critical flow lines and the self-similar solution curves are shown. (*b–d*) Flow is from left to right and the vertical ruler marks the narrowest section. (*b*) Regime (i) plunging flow with $Q_{REL} = 1.03$. (*c*) Regime (iii) plunging flow with $Q_{REL} = 1.26$. (*d*) Regime (iv) plunging flow with $Q_{REL} = 2.00$.

plunge line was not steady. There is intense mixing in the divergent section of the channel. This, coupled with the fairly shallow layer of stagnant fluid, led to considerable circulation in the stagnant layer as fluid from the reservoir moves into the contraction to replace fluid entrained by the instabilities and carried into the reservoir as part of the newly formed mixed region. Again, the mixing involves the stagnant fluid and the upper moving layer, and the lower layer flows into the reservoir unmixed.

In regimes (iii) and (iv), the plunging flows systematically depart from the solutions predicted by the hydraulic theory. The theory predicts that upstream of the plunge point, the flow is self-similar, the layer thicknesses remain constant and so y_1/y_2 is constant. Figures 16(*c*) and 16(*d*) show that upstream of the plunge point, the lower layer thins and since the free surface is approximately level, there is a significant change in the ratio y_1/y_2. This is reflected in figure 16(*a*) – the Froude number of the upper layer is smaller than predicted by the theory owing to the systematic thickening of the upper layer. This results in the data points in figure 16(*a*) being displaced to the left of the $2\frac{1}{2}$-layer self-similar solution curve, whereas the theory of §4, figures 9 and 10, predict that in regimes (iii) and (iv), as the total volume flux increases, the Froude number at the narrowest section will be displaced to the right of this curve, towards the two-layer self-similar solution curve.

Preliminary experiments were conducted in which the configuration of the layers was inverted – two lighter layers were pumped into a denser tank to create regime (iii) and (iv) plunging flows. The 'plunge' was on the bottom of the tank rather than at the free surface and the two moving layers flow over the heavier stagnant fluid in the divergent section of the channel. The upstream deviation from the theoretically predicted level interface was then considerably smaller than in the flows shown in figures 16(*c*) and 16(*d*), but was not completely eliminated.

6. Discussion

The various solutions sets for two-layer flow through a contraction have a number of similar features. Solutions have been plotted in a Froude-number plane that is independent of the density of the stagnant layers. Changing the densities of the layers or removing one or both stagnant layers alters the Froude numbers at which certain features appear but does not affect the underlying structure of the solution set already seen in Armi (1986).

Since the total depth of the moving layers has been allowed to vary, there are always two critical lines in the Froude-number plane. There is always only one solution, the self-similar solution found by Wood (1968), that crosses both critical lines. This is the only solution that originates in a stagnant reservoir and flows through the contraction with both layers dynamically active. The coupling between the two layer is strong and the flow encounters two controls. At lower Froude numbers, the relative thickness of each layer is controlled, and at higher Froude numbers, the total depth of the moving layers is controlled. The position in the Froude-number plane of the higher-Froude-number critical line is quite sensitive to changes in the step between the stagnant and moving layers relative to the density step between the moving layers.

Four plunging flow regimes, defined by the position of the plunge point relative to the positions of the virtual control and the narrowest section, have been identified. For a fixed flow ratio, as the total flow rate is increased, the progression through the first two regimes is accompanied by a change in the upstream reservoir conditions.

At the lowest flow rate, the reservoir conditions are those required by the $2\frac{1}{2}$-layer self-similar solution, and as the flow rate increases, the conditions changes to those required by the two-layer self-similar solution.

A series of laboratory experiments demonstrated the flow of two layers beneath a stagnant layer and a range of two-layer plunging flows. In the divergent section, all of the fully supercritical $2\frac{1}{2}$-layer flows were unstable owing to the shear between the upper moving layer and the overlying stagnant fluid. Instability was also seen in the flow with critical flow upstream of the narrowest section and internally supercritical flow in the divergent section. The stability of internal hydraulic flows, discussed for exchange flows by Lawrence (1990), must be considered when these solutions are applied. At the higher flow rates studied here, non-hydrostatic effects and mixing become important, and the hydraulic theory only provides a qualitative description of the plunging flows. At low and moderate flow rates, the hydraulic theory gives a quantitative description of the observed $2\frac{1}{2}$-layer and plunging flows.

Our research is supported by the Office of Naval Research and the National Science Foundation. We would like to thank the reviewers for many helpful comments on earlier versions of the manuscript.

REFERENCES

ARMI, L. 1986 The hydraulics of two flowing layers with different densities. *J. Fluid Mech.* **163**, 27–58.

ARMI, L. & FARMER, D. M. 1986 Maximal two-layer exchange through a contraction with barotropic flow. *J. Fluid Mech.* **164**, 27–51.

BRYANT, P. J. & WOOD, I. R. 1976 Selective withdrawal from a layered fluid. *J. Fluid Mech.* **77**, 581–591.

FARMER, D. M. & ARMI, L. 1986 Maximal two-layer exchange over a sill and through the combination of a sill and contraction with barotropic flow. *J. Fluid Mech.* **164**, 53–76.

LAI, K. K. & WOOD, I. R. 1975 A two-layer flow through a contraction. *J. Hydraul. Res. IAHR* **13**, 19–34.

LAWRENCE, G. A. 1990 On the hydraulics of Boussinesq and non-Boussinesq two-layer flows. *J. Fluid Mech.* **215**, 457–480.

WOOD, I. R. 1968 Selective withdrawal from a stably stratified fluid. *J. Fluid Mech.* **32**, 209–223.

WOOD, I. R. 1970 A lock exchange flow. *J. Fluid Mech.* **42**, 671–687.